

pubs.acs.org/JACS Article

Engineering Screw Dislocations in Covalent Organic Frameworks

Bhausaheb Dhokale, Kira Coe-Sessions, Michael J. Wenzel, Alathea E. Davies, Taylor Kelsey, Jonathan A. Brant, Laura de Sousa Oliveira, Bruce A. Parkinson, and John O. Hoberg*



Cite This: https://doi.org/10.1021/jacs.4c07859



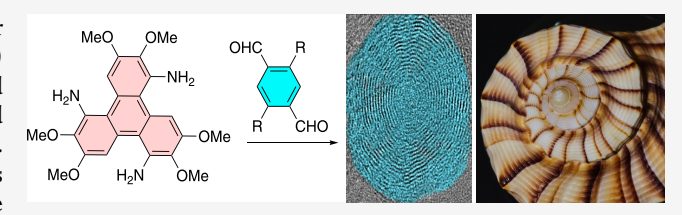
ACCESS I

III Metrics & More

Article Recommendations

Supporting Information

ABSTRACT: We report the application of a Pictet-Spengler reaction to the synthesis of covalent organic frameworks (COFs) using functionalized terephthalaldehydes. The COFs produced show an increased propensity to generate screw dislocations and produce multilayered flakes when compared with other 2D-COFs. Using HRTEM, definitive evidence for screw dislocations was obtained and is presented. The effects on separations using these materials in membranes are also reported.



1. INTRODUCTION

Covalent organic frameworks (COFs) are crystalline materials composed of organic building blocks linked together through covalent bonds, resulting in extended periodic structures. ^{1–3} They have emerged as a versatile class of crystalline, two-dimensional (2D) materials with tunable structures and functionalities, making them attractive candidates for a variety of applications. ^{4,5} Their unique feature lies in their nodal modularity, enabling precise tailoring of properties through rational design and synthesis to influence their mechanical, electrical, and optical properties. 2D-COFs also allow for both variation of size and functionality of the pores, facilitating their use in advanced separation membranes. ^{6–14}

All 2D materials, such as graphene or metal dichalcogenides, exhibit various types and frequency of defects, one being screw dislocations (SDs), 15,16 which can influence the properties of the material. A screw dislocation occurs when there is a linear defect within the atomic arrangement, causing a growing layer to tilt vertically up or down such that as the growth continues, the lattice is distorted in a helical manner around a line axis, like a spiral staircase or a screw. The result is to produce 3D connectivity in a multilayer flake that may be indistinguishable from ordered stacking at distances far from the dislocation. Large numbers of this type of dislocation will obviously influence a COF 2D-stacking structure, 17,18 which in turn can significantly impact the material's properties, mechanical strength, and, particularly its performance in molecular separations as a sorbent or in a membrane. Thus, understanding and controlling screw dislocations in 2D materials is crucial as this can influence material properties for specific applications. Small incidences of SDs often go unnoticed and, therefore, are ignored. However, the use of COFs as separation membranes, as one example, depends on minimizing interlayer flow and constraining solvent through functionalized pores within the COFs, thus enabling the selective separation of complex mixtures. To optimize the separation performance,

COF pores are often functionalized with various functional groups that can be tailored to interact specifically with target molecules, enhancing the membrane's selectivity. Understandably, the inclusion of screw dislocations impacts the stacking behavior of the materials and, therefore, can influence interfacial flow. In this article, we have designed a system that is particularly susceptible to the formation of screw dislocations in order to provide definitive evidence of SDs in a COF and tested their impact on a separation.

The basis of this work is premised on our use of a coronene node for COF construction, 19 which was based on the strategy by Wei et al for the formation of triazacoronenes (TACs) using a 3-fold Pictet-Spengler reaction, Figure 1.^{20–22} The three-step reaction begins with the attack of the triphenylene triamines on substituted benzaldehydes to form imine linkages, followed by electrophilic aromatic cyclization to produce the new ring in yellow. Dehydrogenation under an air atmosphere completes the sequence to form the green bond, leading to the aromatic pyridine ring. As illustrated in the figure, the blue ring is out of plane with the triazacoronene moiety. To our knowledge, only one attempt at polymer formation using the triphenylene node has been reported (R = H), in which Coskun reported its reaction with terephthalaldehyde resulting in an amorphous polymer, as evident from the pXRD.^{23*} Conversely, COF construction via multistep sequences (including initial Schiff base formation) is well established.^{24–40}

With regard to the TAC node in Figure 1, the perpendicular ring (blue) lends itself to lattice rotation such that a helical pattern may be favored. An initial test using atropisomer

Received: June 14, 2024 Revised: September 3, 2024 Accepted: September 9, 2024



Figure 1. Triazacoronene synthesis using a 3-fold Pictet-Spengler reaction.

triazacoronenes was performed first to establish this twisting, followed by COF formation to better observe the induction of screw dislocations in these COFs.

2. RESULTS AND DISCUSSION

Triphenylenes are typically synthesized in three steps from catechol derivatives via Scholl reaction, 41 nitration, 22 and reduction of the trinitro to produce 1 in high yields, Scheme 1. Synthesis of the triaminotriphenylene 1 is easily achieved in 128 g (Scholl), 90 g (nitration), and 3 g (reduction) scales.

Scheme 1. Triphenylene Synthesis

A series of TAC-forming reactions were performed to study the conditions and confirm that the reactions are not impacted by ortho substituents. Triphenylene 1 was heated at 120 °C under an air atmosphere with 2-nitrobenzaldehyde in DMF with triflic acid (TfOH) as a catalyst, Scheme 2. Additionally, 2-aminobenzaldehyde and hydroxyisobenzofuranone (2-formylbenzoic acid) were reacted under similar conditions.

Both NO₂-TAC and CO₂H-TAC were successfully synthesized as red- and orange-yellow-colored solids, respectively; however, attempts on the use of 2-aminobenzaldehyde gave complex mixtures, presumably due to competition from the amine group of aminobenzaldehyde. Therefore, the reduction of the NO2-TAC nitro groups was performed to give NH2-TAC. Characterization of the NO₂-TAC displayed mixtures of both syn and anti atropisomers, as illustrated. These isomers were formed in equal amounts with three nitro groups syn to each other and an anti-isomer in which one nitro was opposite to the other two. This was apparent via ¹H NMR (Figure S7) in which multiple methoxy signals were observed when compared with only two if unsubstituted benzaldehydes were used.²¹ Reduction to NH₂-TAC was initially confirmed via Fourier transform infrared (FTIR) spectroscopy (Figure S12) in which the nitro 1519, 1343, and 786 stretches disappeared,

while the NH₂ appeared at 3434 and 3353 cm⁻¹. Additionally, a single isomer was observed in the ¹H NMR spectrum of NH₂-TAC, as deduced from only two methoxy signals (Figure S13 for comparison spectra). This was also confirmed from the ¹³C NMR spectrum (Figure S11) in which 13 aromatic and two methoxy resonances were observed, i.e., a single isomer. A hydrogen bonded NH₂-TAC, as illustrated in Scheme 2, is proposed in which near planarity is approached. In the characterization of CO₂H-TAC, the ¹H NMR (Figure S14) definitively confirmed the atropisomers with the expected appearance of eight methoxy signals, six from the anti-isomer and two from the syn. Additional verification was obtained from the ¹³C NMR spectrum (Figure S1) in which a very complex set of aromatic resonances appeared.

With conditions and characterization of models in hand, terephthaldehyde nitro and carboxylic acid derivatives were synthesized, as shown in Scheme 3. Only a single nitration could be achieved, resulting in 2-nitroterephthaldehyde 2, regardless of the vast array of conditions attempted. The formation of 2,5-diformylterephthalic acid 3 was achieved by palladium-catalyzed carbonylation of 2,5-dibromoterephthaldehyde. Monomer 3 exists as a mixture of tautomers with the major one being the benzodifuran dione (see SI for characterization of these tautomers and a crystal structure of the difuran). COF formation using these monomers was achieved with triphenylene 1 using the solvothermal procedures established above, which resulted in black solids that were characterized, as discussed below.

Initial indications of successful NO2TAC-COF formation was established using FTIR, which provided strong evidence (Figure S17). Noticeable disappearances of the starting monomers amine (\sim 3395/3320 cm⁻¹) and aldehyde (1690 cm⁻¹) stretches with the appearance of the imine stretch (1615 cm⁻¹) in the COF indicated its formation. Additionally, a strong MeO stretch at 1101 cm⁻¹, nitro stretches at 1526, 1343, and 635 cm⁻¹, with weaker C-H stretches at 2933 cm⁻¹ in the COF further confirmed successful construction. As with the coronene reduction of NO₂TAC, reduction of NO₂TAC-COF to NH₂TAC-COF was also accomplished. Again, FTIR clearly indicated the successful formation of NH2TAC-COF via the disappearance of the above nitro stretches and the appearance of a very broad amine stretch at 3363 cm⁻¹ (Figure S18). The IR of CO₂H TAC-COF (Figure S19) displayed a strong H-bonded OH stretch from 3500 to 2500 cm⁻¹ along

Scheme 2. Triazacoronene Atropisomer Synthesis

with a carbonyl stretch at 1712 cm⁻¹, as compared to the stretch at 1746 cm⁻¹ in monomer 3. A comparison of this COF to its corresponding coronene CO₂H-TAC also corroborates formation as the coronene also displayed the same broad OH along with the carbonyl shift.

High-resolution transmission electron microscopy (HRTEM), Figure 2, provided direct evidence for the extensive formation of screw dislocations. Both rows one and two depict TEM images of NO2, NH2, and CO2H TAC-COFs, respectively. Highlighted in blue in row one is clear evidence of SD in which the NO₂TAC-COF (2A) displayed two SDs. Equally noticeable are the SDs observed in NH₂TAC-COF (2B). This also illustrates that these flakes remain intact after the chemical conversion of the nitro to amines. Most impressive is (2C), which clearly illustrates two distinct spirals and are part of a larger remarkable array of spiral flakes (Figures S20 and 21). The insets in Figure 2C show FFT images of the respective spiral regions, confirming the presence of screw dislocations. Full-page depictions of A and C are provided in Figures S20 and S24, and Figures S22-29 illustrate additional enlarged images, including Figure S25 that has up to 10 observable SDs.

Equally convincing are the electron diffraction patterns of these three COFs depicted in row three in Figure 2. Figure 2I has a nearly identical pattern to previously reported diffraction from screw dislocations in a 2D tungsten disulfide material, 42 in which the inner ring displays a set of hexagonal spots representing one layer and the second set (same inner ring) is the lattice twist angle of the next layer (thus providing the angle from the diffractions spots). Barely visible in this same ring is the third rotation (see Figure S22 for enlargement). Interestingly, the flakes in Figure 2F show no indication of SD but appear to be several nearly identical flakes stacked perfectly upon each other. Thus, SD could easily be overlooked if not for the electron diffraction. Additionally, Figure 2D and E also provide no clear indication of SDs, but these are readily apparent in the diffraction patterns in Figure 2G and H, in which increasing twists lead to the extended pattern in each

ring. Figure 2H particularly shows a broadening of the spots that would indicate a slight shift in the layers above or below due to stacking offsets induced by screw dislocation. Whereas in Figure 2I, a distinct rotation between 2 and 3 layers of COF illustrates the offset of two layers due to a SD. As in other 2D materials and 3D materials with SDs, the lattice may adjust to the presence of SDs at distances remote from the SD.

An in-depth analysis of the flake in Figure 2F was next undertaken and is illustrated in Figure 3. The zoomed-in image of the flake is depicted in Figure 3B with an applied FFT filter displayed in Figure 3C. Notably, this FFT image matches with the experimental SAED image in Figure 2I. Next, the inverse FFT filters of selected points in Figure 3C were obtained and are displayed in Figure 3D–F. The inset shows the selected point in red circles on which the inverse FFT filter was applied. The inverse FFT shows different orientations, indicating different rotations of the 2D sheets. Compared to the 2D COF sheet in Figure 3D, the sheets in Figure 3 E,F are rotated by 22° and 37° angles, respectively.

Powder X-ray diffraction (pXRD) was performed to evaluate the bulk crystallinity of the materials. It is important to note that unlike most COF-forming reactions that involve only a single synthetic step (i.e., imine formation), those reported herein involve the three sequential reactions, as outlined in the Introduction. Furthermore, the second and third steps are predominantly irreversible, and therefore, a more amorphous pXRD was expected. The resulting pXRDs showed broad peaks, as shown in Figure 4. NO₂TAC-COF (green) displayed a reasonably narrow pore spacing peak at 6.9° for the 100 facet and a broad 001 peak (21.8°) for the layer spacing. NH₂TAC-COF (black) produced a similar pXRD (5.2° and 17.6°) and in addition displayed several sharper peaks, presumably from the palladium nanoparticles left over from the reduction (40.2°). CO₂H TAC-COF (red) also displayed similar sharp pore spacing at 6.4° and broad layer spacing at 20.7°. These broad layer spacings are to be expected and are inline with the observed screw dislocations that are intermixed with the 2D flakes and lend further credibility for

Scheme 3. Monomer and Triazacoronene COF Synthesis

SD. Furthermore, calculations for AA, AA slipped, and AB failed to produce matching patterns to the experimental ones (Figures S30-33), which again is expected due to the abundance of SDs that interrupts the periodicity of the lattices.

Finally, the COFs were further characterized using routine techniques including nitrogen BET isotherms, pore size distributions, and thermogravimetric analysis (Figures S34–41), all of which further confirmed the material structure and properties. DSC-TGA revealed a small amount of water loss of ~5% and then a weight loss of ~40% up to 500 °C in which 50–60% of the material was still intact, illustrating the high stability of these materials. Nitrogen adsorption isotherms (BET) for NO₂ and NH₂TAC-COFs displayed a single pore size distribution and confirmed the calculated pore spacings of 17 Å in these two. The CO₂H TAC-COF displayed two major distributions at 6 and 10 Å, which may be a result of a higher percentage of SDs in the material.

An initial design concept was to use the carboxylic acid groups in the CO_2H TAC-COF for separations in light of our previous success using carboxylated COFs in membrane separations. 9,12,43 In these previous studies, excellent separa-

tions were obtained using carboxylated COFs. Given that membrane separations facilitate transport through or rejection of substances by a pore, CO2H TAC-COF ability as a separation membrane could indicate whether there is an impact by SD on separations. Membranes were constructed with the COF supported on a porous anodic aluminum oxide (AAO) filter and placed in a Steritech dead-end permeation cell (see the SI for procedures and results, Figures S44-53). It immediately became evident that the COF was adsorbing the dye (Acid Fushin), which, as reported by Dichtel et al, will occur in particular COFs. 44 Further testing using either acid or basic solutions to adjust Coulombic repulsions also failed to achieve rejection of the dye, indicating that even with chargecharge repulsion of dye to the COF or the use of a dye that is too large to fit through the COF pores, rejection was not feasible. Given these results, the NH2TAC-COF was also tested and it also failed to produce any dye separation (see Figures S54-56). Thus, we conclude that transport through this type of COF is not reliant on passage through a pore but rather on pathways between sheets and grain boundaries, which results in a lack of dye rejection.

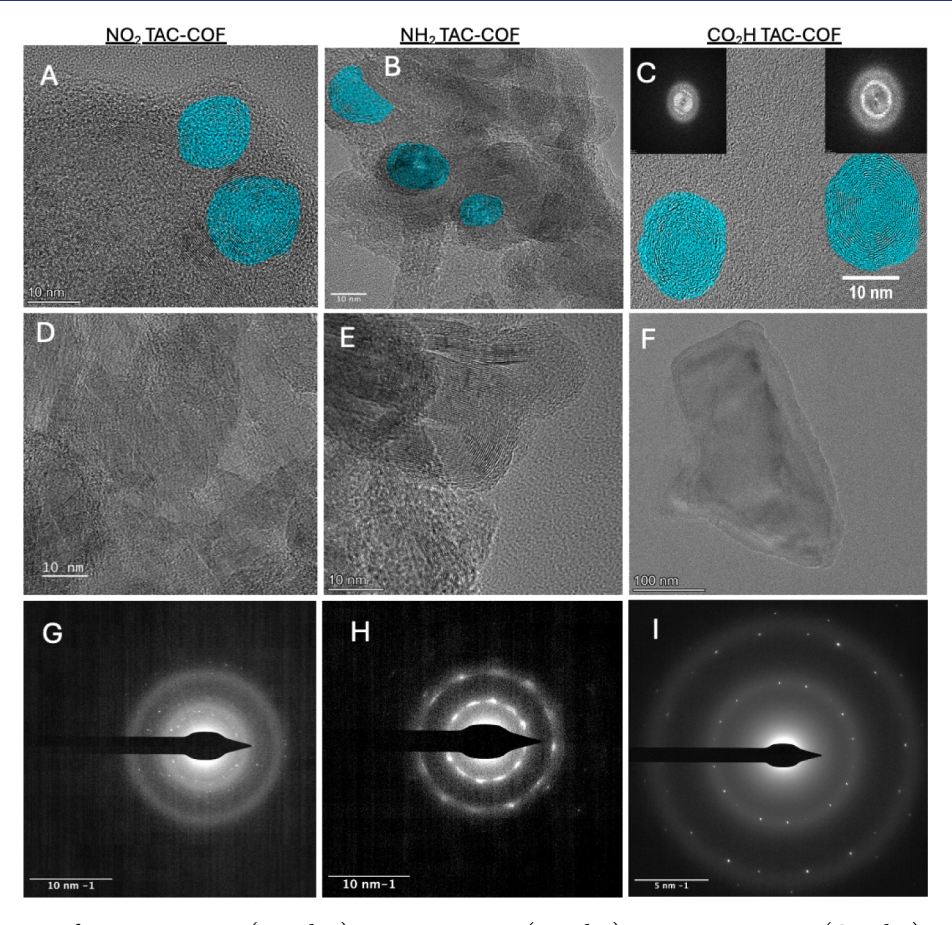


Figure 2. HRTEM images of $NO_2TAC-COF$ (A and D), $NH_2TAC-COF$ (B and E), CO_2H TAC-COF (C and F) and electron diffraction images of $NO_2TAC-COF$ (G), $NH_2TAC-COF$ (H), and CO_2H TAC-COF (I). Each diffraction is from the above row of flakes (D-F).

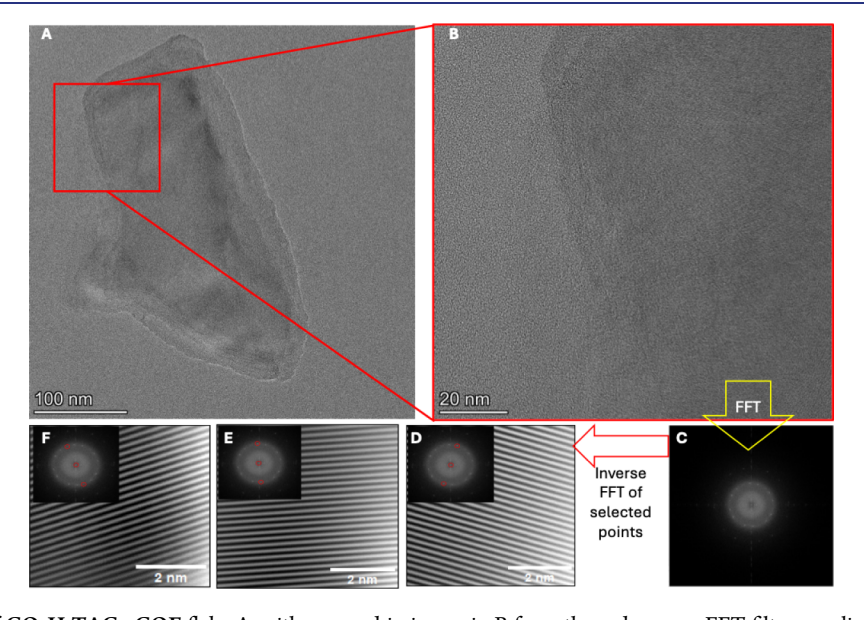


Figure 3. TEM analysis of CO_2H TAC-COF flake A, with zoomed-in image in B from the red square. FFT filters applied on the whole image in B and inverse FFT filters applied on selected spots on C (D-F) illustrating dislocation positions.

3. CONCLUSION

As in all two-dimensional materials, screw dislocations often occur as a growth mechanism, and we have illustrated in this work that covalent organic frameworks are no exception to this generality. The ability of one of the monomers to undergo a lattice rotation, as implemented in this study, leads to an

increased abundance of SD when compared with other 2D-COFs. Although COFs do present a promising platform for the development of advanced separation membranes, SDs will impact stacking in the vertical direction, impacting the configuration and orientation of the layered materials, which as demonstrated in one instance herein impacts separation

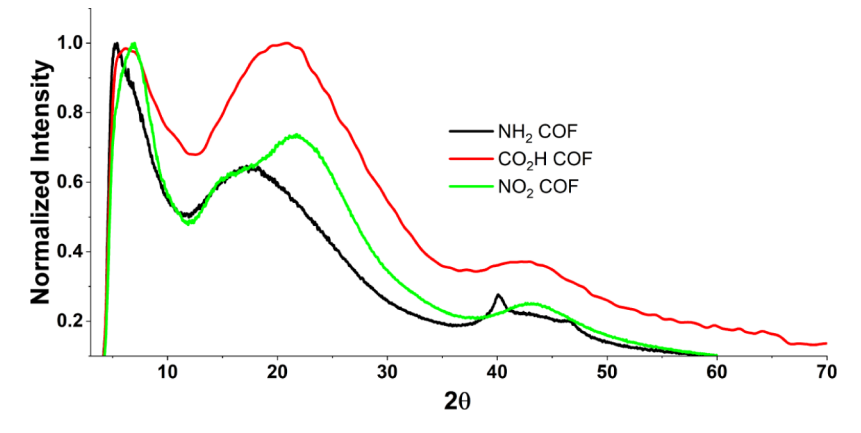


Figure 4. pXRD of NO₂TAC-COF (green), CO₂H TAC-COF (red), and NH₂TAC-COF (black).

abilities and efficiencies. While screw dislocation—driven growth has been largely ignored in the COF community, it is imperative that those developing COF-based separation technologies and other applications be mindful of its occurrence and inclusion in the materials. Alternatively, screw-dislocated layered COFs may have interesting properties in numerous other areas that may prove to be fitting for exploration.

ASSOCIATED CONTENT

Solution Supporting Information

The Supporting Information is available free of charge at https://pubs.acs.org/doi/10.1021/jacs.4c07859.

All experimental and characterization data for the synthesis of starting monomers and COFs, including mass spectrometry, NMR, IR, XRD, TEM data, DSC-TGA, and computational methods (PDF)

Accession Codes

CCDC 2359077 contains the supplementary crystallographic data for this paper. These data can be obtained free of charge via www.ccdc.cam.ac.uk/data_request/cif, or by emailing data_request@ccdc.cam.ac.uk, or by contacting the Cambridge Crystallographic Data Centre, 12 Union Road, Cambridge CB2 1EZ, UK; fax: +44 1223 336 033.

AUTHOR INFORMATION

Corresponding Author

John O. Hoberg – Department of Chemistry, University of Wyoming, Laramie, Wyoming 82071, United States; orcid.org/0000-0003-3833-8122; Email: hoberg@uwyo.edu

Authors

Bhausaheb Dhokale — Department of Chemistry, University of Wyoming, Laramie, Wyoming 82071, United States;
ocid.org/0000-0001-7520-4727

Kira Coe-Sessions — Department of Chemistry, University of Wyoming, Laramie, Wyoming 82071, United States

Michael J. Wenzel — Department of Chemistry, University of Wyoming, Laramie, Wyoming 82071, United States

Alathea E. Davies — Department of Chemistry, University of Wyoming, Laramie, Wyoming 82071, United States

Taylor Kelsey — Department of Chemistry, University of Wyoming, Laramie, Wyoming 82071, United States

Jonathan A. Brant — Department of Civil Engineering, University of Wyoming, Laramie, Wyoming 82071, United States

Laura de Sousa Oliveira — Department of Chemistry, University of Wyoming, Laramie, Wyoming 82071, United States

Bruce A. Parkinson — Department of Chemistry, University of Wyoming, Laramie, Wyoming 82071, United States;
orcid.org/0000-0002-8950-1922

Complete contact information is available at: https://pubs.acs.org/10.1021/jacs.4c07859

Author Contributions

The manuscript was written through contributions of all authors. All authors have given approval to the final version of the manuscript.

Funding

NSF DMREF grant #2118592 and the UW Center of Energy Materials.

Notes

The authors declare no competing financial interest.

ACKNOWLEDGMENTS

The authors acknowledge generous support from NSF DMREF grant #2118592 and the UW Center of Energy Materials. The authors would also like to acknowledge the use of computational resources at the NCAR-Wyoming Supercomputing Center provided by the National Science Foundation and the State of Wyoming and supported by NCAR's Computational and Information Systems Laboratory (Project WYOM0145),⁴⁵ and the Advanced Research Computing Center, Beartooth Computing Environment at the University of Wyoming.⁴⁶ Crystal structure analysis was performed by Arulsamy Navamoney, and assistance with TEM imaging was provided by Qian Yang.

REFERENCES

- (1) Geng, K.; He, T.; Liu, R.; Dalapati, S.; Tan, K. T.; Li, Z.; Tao, S.; Gong, Y.; Jiang, Q.; Jiang, D. Covalent Organic Frameworks: Design, Synthesis, and Functions. *Chem. Rev.* **2020**, *120* (16), 8814–8933.
- (2) Jiang, J.; Zhao, Y.; Yaghi, O. M. Covalent Chemistry beyond Molecules. J. Am. Chem. Soc. 2016, 138 (10), 3255–3265.
- (3) Lohse, M. S.; Bein, T. Covalent Organic Frameworks: Structures, Synthesis, and Applications. *Adv. Funct. Mater.* **2018**, 28 (33), 1705553.

- (4) Tan, K. T.; Ghosh, S.; Wang, Z.; Wen, F.; Rodríguez-San-Miguel, D.; Feng, J.; Huang, N.; Wang, W.; Zamora, F.; Feng, X.; Thomas, A.; Jiang, D. Covalent Organic Frameworks. *Nat. Rev. Methods Primers* **2023**, 3 (1), 1.
- (5) Song, Y.; Sun, Q.; Aguila, B.; Ma, S. Opportunities of Covalent Organic Frameworks for Advanced Applications. *Adv. Sci.* **2019**, *6* (2), 1801410.
- (6) Wang, Z.; Zhang, S.; Chen, Y.; Zhang, Z.; Ma, S. Covalent Organic Frameworks for Separation Applications. *Chem. Soc. Rev.* **2020**, 49 (3), 708–735.
- (7) Yuan, S.; Li, X.; Zhu, J.; Zhang, G.; Van Puyvelde, P.; Van Der Bruggen, B. Covalent Organic Frameworks for Membrane Separation. *Chem. Soc. Rev.* **2019**, *48* (10), 2665–2681.
- (8) Spaulding, V.; Zosel, K.; Duong, P. H. H.; Li-Oakey, K. D.; Parkinson, B. A.; Gomez-Gualdron, D. A.; Hoberg, J. O. A Self-Assembling, biporous, Metal-Binding Covalent Organic Framework and Its Application for Gas Separation. *Mater. Adv.* **2021**, 2 (10), 3362–3369.
- (9) Kuehl, V. A.; Yin, J.; Duong, P. H. H.; Mastorovich, B.; Newell, B.; Li-Oakey, K. D.; Parkinson, B. A.; Hoberg, J. O. A Highly Ordered Nanoporous, Two-Dimensional Covalent Organic Framework with Modifiable Pores, and Its Application in Water Purification and Ion Sieving. *J. Am. Chem. Soc.* 2018, 140 (51), 18200–18207.
- (10) Kuehl, V. A.; Wenzel, M. J.; Parkinson, B. A.; de Sousa Oliveira, L.; Hoberg, J. O. Pitfalls in the Synthesis of Polyimide-Linked Two-Dimensional Covalent Organic Frameworks. *J. Mater. Chem. A* **2021**, 9 (27), 15301–15309.
- (11) Kuehl, V. A.; Duong, P. H. H.; Sadrieva, D.; Amin, S. A.; She, Y.; Li-Oakey, K. D.; Yarger, J. L.; Parkinson, B. A.; Hoberg, J. O. Synthesis, Postsynthetic Modifications, and Applications of the First Quinoxaline-Based Covalent Organic Framework. *ACS Appl. Mater. Interfaces* **2021**, *13*, 37494–37499.
- (12) Duong, P. H. H.; Shin, Y. K.; Kuehl, V. A.; Afroz, M. M.; Hoberg, J. O.; Parkinson, B.; van Duin, A. C. T.; Li-Oakey, K. D. Mechanistic Study of pH Effect on Organic Solvent Nanofiltration Using Carboxylated Covalent Organic Framework as a Modeling and Experimental Platform. Sep. Purif. Technol. 2022, 282, 120028.
- (13) Duong, P. H. H.; Shin, Y. K.; Kuehl, V. A.; Afroz, M. M.; Hoberg, J. O.; Parkinson, B. A.; van Duin, A. C. T.; Li-Oakey, K. D. Molecular Interactions and Layer Stacking Dictate Covalent Organic Framework Effective Pore Size. ACS Appl. Mater. Interfaces 2021, 13, 42164–42175
- (14) Brophy, J.; Summerfield, K.; Yin, J.; Kephart, J.; Stecher, J.; Adams, J.; Yanase, T.; Brant, J.; Li-Oakey, K.; Hoberg, J.; Parkinson, B. The Influence of Disorder in the Synthesis, Characterization and Applications of a Modifiable Two-Dimensional Covalent Organic Framework. *Materials* **2021**, *14* (1), 71.
- (15) Zhao, Y.; Jin, S. Stacking and Twisting of Layered Materials Enabled by Screw Dislocations and Non-Euclidean Surfaces. *Acc. Mater. Res.* **2022**, *3* (3), 369–378.
- (16) Meng, F.; Morin, S. A.; Forticaux, A.; Jin, S. Screw Dislocation Driven Growth of Nanomaterials. *Acc. Chem. Res.* **2013**, 46 (7), 1616–1626.
- (17) Pütz, A. M.; Terban, M. W.; Bette, S.; Haase, F.; Dinnebier, R. E.; Lotsch, B. V. Total Scattering Reveals the Hidden Stacking Disorder in a 2D Covalent Organic Framework. *Chem. Sci.* **2020**, *11* (47), 12647–12654.
- (18) Nguyen, V.; Grünwald, M. Microscopic Origins of Poor Crystallinity in the Synthesis of Covalent Organic Framework COF-5. *J. Am. Chem. Soc.* **2018**, *140* (9), 3306–3311.
- (19) Coe-Sessions, K.; Davies, A. E.; Dhokale, B.; Wenzel, M. J.; Gahrouei, M. M.; Vlastos, N.; Klaassen, J.; Parkinson, B. A.; De Sousa Oliveira, L.; Hoberg, J. O. Functionalized Graphene via a One Pot Reaction Enabling Exact Pore Sizes, Modifiable Pore Functionalization and Precision Doping *J. Am. Chem. Soc.* **2024**, DOI: 10.1021/jacs.4c10529
- (20) Wei, J.; Han, B.; Guo, Q.; Shi, X.; Wang, W.; Wei, N. 1,5,9-Triazacoronenes: A Family of Polycyclic Heteroarenes Synthesized by

- a Threefold Pictet-Spengler Reaction. Angew. Chem., Int. Ed. 2010, 49 (44), 8209–8213.
- (21) Sun, Y.; Wang, X.; Shen, G.; Yang, T.; Yang, Y.; Li, J.; Yang, M.; Sun, H.; Wei, J. A 6π Azaelectrocyclization Strategy towards the 1,5,9-Triazacoronenes. *Adv. Synth. Catal.* **2020**, 362 (8), 1651–1656.
- (22) Liu, B.; Shi, D.; Yang, Y.; Liu, D.; Li, M.; Liu, E.; Wang, X.; Zhang, Q.; Yang, M.; Li, J.; Shi, X.; Wang, W.; Wei, J. Triazacoronene Derivatives with Three *Peri* -Benzopyrano Extensions: Synthesis, Structure, and Properties: Triazacoronene Derivatives with Three *Peri* -Benzopyrano Extensions: Synthesis, Structure, and Properties. *Eur. J. Org. Chem.* **2018**, 2018 (7), 869–873.
- (23) Lee, J.; Buyukcakir, O.; Kwon, T.; Coskun, A. Energy Band-Gap Engineering of Conjugated Microporous Polymers via Acidity-Dependent in Situ Cyclization. *J. Am. Chem. Soc.* **2018**, *140* (35), 10937–10940.
- (24) Cusin, L.; Peng, H.; Ciesielski, A.; Samorì, P. Chemical Conversion and Locking of the Imine Linkage: Enhancing the Functionality of Covalent Organic Frameworks. *Angew. Chem., Int. Ed.* **2021**, *60* (26), 14236–14250.
- (25) Das, P.; Chakraborty, G.; Roeser, J.; Vogl, S.; Rabeah, J.; Thomas, A. Integrating Bifunctionality and Chemical Stability in Covalent Organic Frameworks via One-Pot Multicomponent Reactions for Solar-Driven H ₂ O ₂ Production. *J. Am. Chem. Soc.* **2023**, *145* (5), 2975–2984.
- (26) Grunenberg, L.; Savasci, G.; Terban, M. W.; Duppel, V.; Moudrakovski, I.; Etter, M.; Dinnebier, R. E.; Ochsenfeld, C.; Lotsch, B. V. Amine-Linked Covalent Organic Frameworks as a Platform for Postsynthetic Structure Interconversion and Pore-Wall Modification. *J. Am. Chem. Soc.* **2021**, *143* (9), 3430–3438.
- (27) Guo, J.; Xu, Y.; Jin, S.; Chen, L.; Kaji, T.; Honsho, Y.; Addicoat, M. A.; Kim, J.; Saeki, A.; Ihee, H.; Seki, S.; Irle, S.; Hiramoto, M.; Gao, J.; Jiang, D. Conjugated Organic Framework with Three-Dimensionally Ordered Stable Structure and Delocalized π Clouds. *Nat. Commun.* **2013**, 4 (1), 2736.
- (28) Haase, F.; Troschke, E.; Savasci, G.; Banerjee, T.; Duppel, V.; Dörfler, S.; Grundei, M. M. J.; Burow, A. M.; Ochsenfeld, C.; Kaskel, S.; Lotsch, B. V. Topochemical Conversion of an Imine- into a Thiazole-Linked Covalent Organic Framework Enabling Real Structure Analysis. *Nat. Commun.* **2018**, *9* (1), 2600.
- (29) Li, X.; Zhang, C.; Cai, S.; Lei, X.; Altoe, V.; Hong, F.; Urban, J. J.; Ciston, J.; Chan, E. M.; Liu, Y. Facile Transformation of Imine Covalent Organic Frameworks into Ultrastable Crystalline Porous Aromatic Frameworks. *Nat. Commun.* **2018**, *9* (1), 2998.
- (30) Li, X.-T.; Zou, J.; Wang, T.-H.; Ma, H.-C.; Chen, G.-J.; Dong, Y.-B. Construction of Covalent Organic Frameworks via Three-Component One-Pot Strecker and Povarov Reactions. *J. Am. Chem. Soc.* **2020**, *142* (14), 6521–6526.
- (31) Liu, H.; Chu, J.; Yin, Z.; Cai, X.; Zhuang, L.; Deng, H. Covalent Organic Frameworks Linked by Amine Bonding for Concerted Electrochemical Reduction of CO2. *Chem* **2018**, 4 (7), 1696–1709.
- (32) Liu, J.; Yang, T.; Wang, Z.-P.; Wang, P.-L.; Feng, J.; Ding, S.-Y.; Wang, W. Pyrimidazole-Based Covalent Organic Frameworks: Integrating Functionality and Ultrastability via Isocyanide Chemistry. *J. Am. Chem. Soc.* **2020**, *142* (50), 20956–20961.
- (33) Segura, J. L.; Mancheño, M. J.; Zamora, F. Covalent Organic Frameworks Based on Schiff-Base Chemistry: Synthesis, Properties and Potential Applications. *Chem. Soc. Rev.* **2016**, 45 (20), 5635–5671.
- (34) Vitaku, E.; Gannett, C. N.; Carpenter, K. L.; Shen, L.; Abruña, H. D.; Dichtel, W. R. Phenazine-Based Covalent Organic Framework Cathode Materials with High Energy and Power Densities. *J. Am. Chem. Soc.* **2020**, *142* (1), 16–20.
- (35) Waller, P. J.; AlFaraj, Y. S.; Diercks, C. S.; Jarenwattananon, N. N.; Yaghi, O. M. Conversion of Imine to Oxazole and Thiazole Linkages in Covalent Organic Frameworks. *J. Am. Chem. Soc.* **2018**, 140 (29), 9099–9103.
- (36) Waller, P. J.; Lyle, S. J.; Osborn Popp, T. M.; Diercks, C. S.; Reimer, J. A.; Yaghi, O. M. Chemical Conversion of Linkages in

- Covalent Organic Frameworks. J. Am. Chem. Soc. 2016, 138 (48), 15519–15522.
- (37) Wang, K.; Jia, Z.; Bai, Y.; Wang, X.; Hodgkiss, S. E.; Chen, L.; Chong, S. Y.; Wang, X.; Yang, H.; Xu, Y.; Feng, F.; Ward, J. W.; Cooper, A. I. Synthesis of Stable Thiazole-Linked Covalent Organic Frameworks via a Multicomponent Reaction. *J. Am. Chem. Soc.* **2020**, 142 (25), 11131–11138.
- (38) Wang, P.-L.; Ding, S.-Y.; Zhang, Z.-C.; Wang, Z.-P.; Wang, W. Constructing Robust Covalent Organic Frameworks via Multicomponent Reactions. *J. Am. Chem. Soc.* **2019**, *141* (45), 18004–18008
- (39) Yang, Y.; Yu, L.; Chu, T.; Niu, H.; Wang, J.; Cai, Y. Constructing Chemical Stable 4-Carboxyl-Quinoline Linked Covalent Organic Frameworks via Doebner Reaction for Nanofiltration. *Nat. Commun.* **2022**, *13* (1), 2615.
- (40) Zhu, Y.; Huang, D.; Wang, W.; Liu, G.; Ding, C.; Xiang, Y. Sequential Oxidation/Cyclization of Readily Available Imine Linkages to Access Benzoxazole-Linked Covalent Organic Frameworks. *Angew. Chem., Int. Ed.* **2024**, 63 (11), No. e202319909.
- (41) Naarmann, H.; Hanack, M.; Mattmer, R. A High Yield Easy Method for the Preparation of Alkoxy-Substituted Triphenylenes. *Synthesis* **1994**, *1994* (5), 477–478.
- (42) Zhao, Y.; Zhang, C.; Kohler, D. D.; Scheeler, J. M.; Wright, J. C.; Voyles, P. M.; Jin, S. Supertwisted Spirals of Layered Materials Enabled by Growth on Non-Euclidean Surfaces. *Science* **2020**, *370* (6515), 442–445.
- (43) Duong, P. H. H.; Kuehl, V. A.; Mastorovich, B.; Hoberg, J. O.; Parkinson, B. A.; Li-Oakey, K. D. Carboxyl-Functionalized Covalent Organic Framework as a Two-Dimensional Nanofiller for Mixed-Matrix Ultrafiltration Membranes. *J. Membr. Sci.* 2019, 574, 338–348.
- (44) Fenton, J. L.; Burke, D. W.; Qian, D.; Olvera de la Cruz, M.; Dichtel, W. R. Polycrystalline Covalent Organic Framework Films Act as Adsorbents, Not Membranes. *J. Am. Chem. Soc.* **2021**, *143* (3), 1466–1473.
- (45) Computational and Information Systems Laboratory, Cheyenne: HPE/SGI ICE XA System (NCAR Community Computing); National Center of Atmospheric Research: Boulder, CO, 2019.
- (46) Advanced Research Computing Center. Beartooth Computing Environment, X86_64 Cluster; University of Wyoming: Laramie, WY, 2023.